


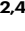

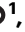
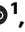





Photonic-electronic integrated circuit-based coherent LiDAR engine

Received: 22 August 2023

Accepted: 2 April 2024

Published online: 11 April 2024

 Check for updates


Anton Lukashchuk ^{1,4}, Halil Kerim Yildirim ^{2,4}, Andrea Bancora ¹, Grigory Lihachev¹, Yang Liu ¹, Zheru Qiu ¹, Xinru Ji¹, Andrey Voloshin¹, Sunil A. Bhave ³, Edoardo Charbon ²  & Tobias J. Kippenberg ¹ 

Chip-scale integration is a key enabler for the deployment of photonic technologies. Coherent laser ranging or FMCW LiDAR, a perception technology that benefits from instantaneous velocity and distance detection, eye-safe operation, long-range, and immunity to interference. However, wafer-scale integration of these systems has been challenged by stringent requirements on laser coherence, frequency agility, and the necessity for optical amplifiers. Here, we demonstrate a photonic-electronic LiDAR source composed of a micro-electronic-based high-voltage arbitrary waveform generator, a hybrid photonic circuit-based tunable Vernier laser with piezoelectric actuators, and an erbium-doped waveguide amplifier. Importantly, all systems are realized in a wafer-scale manufacturing-compatible process comprising III-V semiconductors, silicon nitride photonic integrated circuits, and 130-nm SiGe bipolar complementary metal-oxide-semiconductor (CMOS) technology. We conducted ranging experiments at a 10-meter distance with a precision level of 10 cm and a 50 kHz acquisition rate. The laser source is turnkey and linearization-free, and it can be seamlessly integrated with existing focal plane and optical phased array LiDAR approaches.

Laser ranging (LiDAR) is a widespread perception technology that is rapidly developing using recent progress in silicon photonics^{1–3}. LiDAR is ubiquitous in robotics, spatial mapping, and AR/VR applications and gained popularity in the early 2000s as a key enabler of autonomous vehicles in urban environments, a goal highlighted by DARPA Grand Challenges⁴. Widely employed in the early 2000's time-of-flight sensors, which measure the arrival time of reflected pulses, relied on available legacy 900 nm diode lasers and silicon detectors. Another type of LiDAR is frequency-modulated continuous wave (FMCW) LiDAR^{5,6}, which maps the distance and velocity of an object to frequency. This method, an optical analogue of coherent RADAR, utilizes optical self-heterodyne detection of a frequency-chirped continuous-wave light reflected from a target with its replica, that serves as the local oscillator (LO). In contrast to the time-of-flight approach, coherent ranging allows for instantaneous velocity measurement via

the Doppler frequency shift, quantum noise limited detection enabled by heterodyne detection with sufficient LO power, eye-safe operation at low average powers, immunity to ambient light sources, and low-bandwidth receiver electronics (100s of MHz) capable of providing cm-level resolution mainly dependent on frequency excursion of the transmitted chirp. However, the cost and bulky size of individual LiDAR components and their assembly still preclude the wide adoption of ranging sensors.

Frequency-modulated continuous wave LiDAR, in particular, requires multiple building blocks, including a frequency-agile laser, driving electronics, scanning optics, passive components (grating couplers, switching network), and detectors. A variety of recent work attempted to integrate coherent LiDAR components on chip. Martin et al. demonstrated a silicon photonic circuit with integrated detectors, waveform calibration and switching network for passive beam

¹Institute of Physics, Swiss Federal Institute of Technology Lausanne (EPFL), CH-1015 Lausanne, Switzerland. ²Advanced Quantum Architecture Laboratory (AQUA), Swiss Federal Institute of Technology Lausanne (EPFL), CH-2002 Neuchâtel, Switzerland. ³OxideMEMS Lab, Purdue University, 47907 West Lafayette, IN, USA. ⁴These authors contributed equally: Anton Lukashchuk, Halil Kerim Yildirim.  e-mail: edoardo.charbon@epfl.ch; tobias.kippenberg@epfl.ch

scanning capable of 60 m coherent ranging at 5 mW output power⁷. A number of recent works employed optical phased array (OPA) technology to achieve 2D passive scanning^{8–10}. Poulton et al. demonstrated a nearly centimeter scale OPA aperture with 8192 elements achieving $100^\circ \times 17^\circ$ field of view³. Rogers et al. developed a focal plane array (FPA) 3D LiDAR on a silicon chip with photonic-electronic monolithic integration of a 512-pixel coherent receiver array¹. Further large scaling of FPA pixels employing switchable MEMS grating antennas was reported by Zhang et al.¹¹.

The aforementioned approaches are CMOS compatible, can be integrated with other passive or active optical components and are scalable, i.e., support a further increase in the number of pixels and field of view. However, these prior demonstrations all used external lasers coupled via fiber, off-the-shelf driving electronics, and bulk fiber-based erbium-doped amplifiers for signal or reflection amplification and bulk modulators (Refs. 1,8,12) - significantly compounding full integration. A fully integrated FMCW LiDAR will require to address the remaining integration and replace these building blocks with their photonic integrated circuit-based counterparts. Tackling the issue of discrete external components, Isaac et al. fabricated an integrated transceiver module on the InP platform¹³, but no coherent ranging functionality was performed. Ref. 14 showed a fully integrated coherent LiDAR on the chip, though it is limited to single-pixel imaging only. Here, we make a step further towards fully photonic-electronic integrated LiDAR presenting an integrated laser, high-voltage arbitrary waveform generator (HV-AWG) application-specific integrated circuit (ASIC), and chip-scale Erbium-doped waveguide amplifier (EDWA) - key components for integrated LiDAR source - which are all fabricated with foundry compatible wafer scale manufacturing. Using these photonic integrated circuit-based components we demonstrated ranging at 10 m with cm-level precision. The combination of integrated laser, HV-AWG ASIC and chip-scale Erbium amplifier constitutes a robust, coherent LiDAR source, which can be applied to existing silicon imaging 3D sensors^{1,2,12} and pave a path towards a fully integrated coherent LiDAR system.

Results

Photonic-electronic LiDAR source

The photonic-electronic LiDAR consists (cf. Fig. 1a) of three main building blocks: laser, ASIC, and on-chip amplifier. Generally, a distributed feedback laser (DFB) is used as the light source in FMCW LiDAR implementations^{15–17}. While DFB lasers offer tunability with MHz actuation bandwidth and excursions up to 100s of GHz, they suffer from the need for continuous feedback for chirp linearity¹⁸ - the linearity-phase noise and wide tunability trade-off inherent to conventional lasers¹⁹. Recent advances in integrated photonics have enabled to achieve fiber laser coherence, by using self-injection locking of a DFB laser to ultra-low propagation loss photonic integrated circuits based on silicon nitride²⁰. By endowing such circuits with piezoelectrical MEMS actuators, it has been possible to achieve both high coherence as well as fast tuning with low nonlinearity²¹, allowing linearization-free FMCW LiDAR - yet requiring large voltage driving. Other approaches based on electro-optic integrated photonic laser feedback circuits using $\chi^{(2)}$ materials, such as lithium niobate (LiNbO₃) or barium titanate (BTO)^{22–24} can lead to even faster frequency chirps at a lower voltage, but presently exhibit far lower laser coherence. We note Zhang et al.²⁵ have recently demonstrated that such materials exhibit significantly lower levels of cavity noise at high offset frequencies and are predominantly limited by thermal-charge-carrier-refractive noise.

In our work, we employ a Vernier ring filter-based external cavity hybrid integrated laser²⁶. Such laser configuration has advanced in recent years demonstrating low linewidth^{26,27}, fast tuning²² and implementations on different platforms²². We acknowledge the existence of alternative approaches utilizing ring self-injection locking,

Bragg gratings, (extended) distributed Bragg reflectors, and vertical cavity surface emitting lasers. Performance comparison of these lasers is summarized elsewhere (Supplementary material^{21,28}).

The laser (cf. Fig. 1c) operates at 1566 nm and includes a reflective semiconductor optical amplifier (RSOA) edge-coupled to a Si₃N₄ photonic integrated circuit with a microresonator-based Vernier filter. This approach has the distinct advantage of using cost-effective III-V based RSOA, that does not require gratings as in the case of DFB. Two microresonators with loaded cavity linewidths of 200 MHz slightly differ in free spectral range (FSR), i.e., 96.7 GHz and 97.9 GHz with Vernier frequency of 8.7 THz. Both rings have integrated microheaters realized in the bottom Pt electrode layer. We aligned the pair of resonances using a microheater and obtained up to 20% reflection back to the RSOA, using the feedback circuit depicted in Fig. 1a. Microheaters provide at least 100 GHz continuous cavity frequency tuning, which results in $FSR^2/\Delta FSR \approx 60$ nm discrete laser frequency tuning by matching the resonances of the Vernier ring filter and adjusting the intracavity phase²⁹. Piezoelectric lead zirconate titanate (PZT) actuators were heterogeneously integrated on top of the microrings to perform fast actuation via stress-optic effect for rapid laser frequency tuning. We note that PZT can be monolithically integrated on silicon in a standard CMOS foundry process³⁰. Platinum electrodes (cf. Fig. 1d) match the resonator radius to maximize the stress-optic tuning efficiency, attaining -130 MHz/V of frequency tuning. We note that decreasing the radius of the microring with the PZT actuator improves the tuning efficiency up to 500 MHz/V as reported in²¹. When coupling the hybrid MEMS-based circuit to an RSOA, we observe lasing with an output power of 3 mW, side mode suppression ratio of 50 dB, and featuring frequency noise of 10^4 Hz²/Hz at 10 kHz offset frequency, reaching the white noise floor of 127 Hz²/Hz at 6 MHz offset²⁹. For better stability, the entire assembly is packaged within a butterfly 14-pin package and placed on a Peltier element, and light is coupled to a SMF output fiber. The RSOA, Peltier element, thermistor, all microheaters, and PZT actuators are all connected to the butterfly pins using electrical wirebonding. The hybrid packaging allows for turnkey laser operation, reduces laser frequency noise at offsets below 1 kHz and maintains the tuning performance after waveform predistortion and linearization.

Operating the laser in FMCW mode (cf. Fig. 1b) requires frequency tuning over several GHz, which for PZT integrated actuators necessitates voltages above 10 V, not achievable with conventional CMOS electronics. Moreover, conventional linear modulation laser tuning necessitates feedback to keep the waveform linear. It originates from the non-linear current tuning and electro-optical transduction. The optoelectronic feedback loop is usually utilized to lock the optical chirp detected via delay interferometer to an electronic reference^{18,31}. Other techniques involve preliminary iterative predistortion and linearization of the waveform^{17,21} or resampling of the recorded signal, all of which rely on auxiliary interferometers^{32,33}. To eliminate the necessity for feedback or post-processing and overcome the voltage budget limitation, we designed and fabricated, a HV-AWG integrated circuit (see Fig. 1e) that generates a 20 V sawtooth waveform that drives the PZT actuators while being supplied with only 3.3 V. The electrical waveform is then transduced to the optical domain, resulting in a >2 GHz optical chirp excursion.

FMCW LiDAR can be implemented in various ways. Typically, it uses a triangularly chirped waveform³⁴, but can also use random phase code modulation³⁵. Figure 1b shows the chirp waveform employed in our experiments. Linearly frequency-chirped laser light is split into a local oscillator path and signal path, with the signal path sent to the target. The reflected light is then mixed with the local oscillator and measured on a balanced photodiode. The detected range is proportional to the beatnote frequency inferred from the short-time Fourier transform of the recorded heterodyne signal. It is inversely

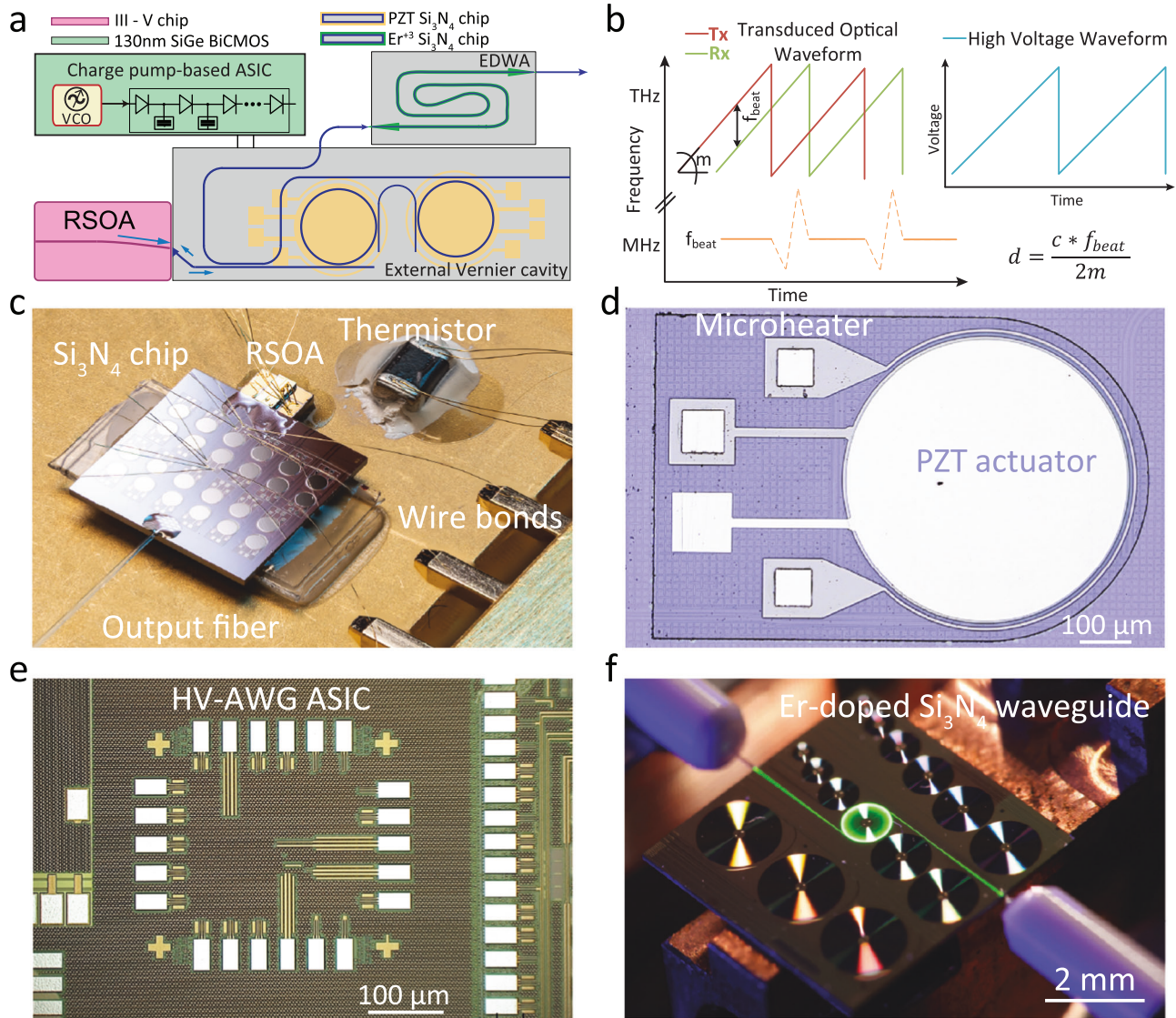


Fig. 1 | Concept of photonic-electronic LiDAR source. **a** Schematics of photonic-electronic LiDAR structure comprising a hybrid integrated laser source, charge-pump based HV-AWG ASIC, photonic integrated erbium-doped waveguide amplifier. **b** Coherent ranging principle. **c** Packaged laser source. RSOA is edge coupled to Si_3N_4 Vernier filter configuration waveguide, whereas the output is glued to the fiber port. PZT and microheater actuators are wirebonded as well as butterfly

package thermistor. **d** Zoom-in view of (c) highlighting a microring with actuators. **e** Micrograph of the HV-AWG ASIC chip fabricated in a 130 nm SiGe BiCMOS technology. The total size of the chip is 1.17–1.07 mm². **f** The Erbium-doped waveguide is optically excited by a 1480 nm pump showing green luminescence due to the transition from a higher lying energy level to the ground state.

proportional to the waveform chirp rate m - the ratio of the frequency excursion and sweeping period.

Finally, we employed a chip-scale integrated EDWA (cf. Fig. 1f) to amplify the laser to >20 mW optical power to meet the power requirements for robust and long-range coherent ranging³⁶. Typically integrated LiDAR systems require >100 mW of optical power to compensate for coupling losses and be able to emit 10s mW at the aperture^{3,7}. The EDWA was implemented using an on-chip 21-cm-long Si_3N_4 spiral waveguide doped with high-concentration Erbium ions (3.25×10^{20} ions/cm) through a high-energy (up to 2 MeV) ion implantation process^{37,38}. The doped Erbium ions can be optically pumped to the excited state and allow for amplification stemming from the stimulated transition to the ground state. The EDWA provides linear and low noise optical amplification to the frequency-modulated optical waveform due to the slow gain dynamics (millisecond lifetime) and the small emission cross section of Erbium ions³⁹.

High-voltage Arbitrary Waveform Generator ASIC

Arbitrary waveform generation at high voltages is desired to drive various devices, including ultrasound transducers^{40,41}, piezoactuators²¹, neurostimulators⁴², single-photon avalanche diodes (SPADs)⁴³. HV-AWGs are usually provided as single or even multiple discrete components^{21,44}, which are generally challenging to integrate due to their incompatibility with technologies supporting advanced electronics. We demonstrate a novel architecture, which can generate high-voltage arbitrary waveforms using a standard CMOS technology supplied at 3.3 V. Figure 2a shows the schematic block diagram of the IC. The ASIC consists of a voltage-controlled ring oscillator (VCRO), which drives the clocks of a series of Dickson charge pump stages. The oscillation frequency can be controlled externally to modify the waveform. The 11-stage charge pump generates the output waveform rising edges, whereas the 15-stage charge pump generates falling edges. The two charge pump blocks operate in a complementary fashion, with the ‘Select’ signal

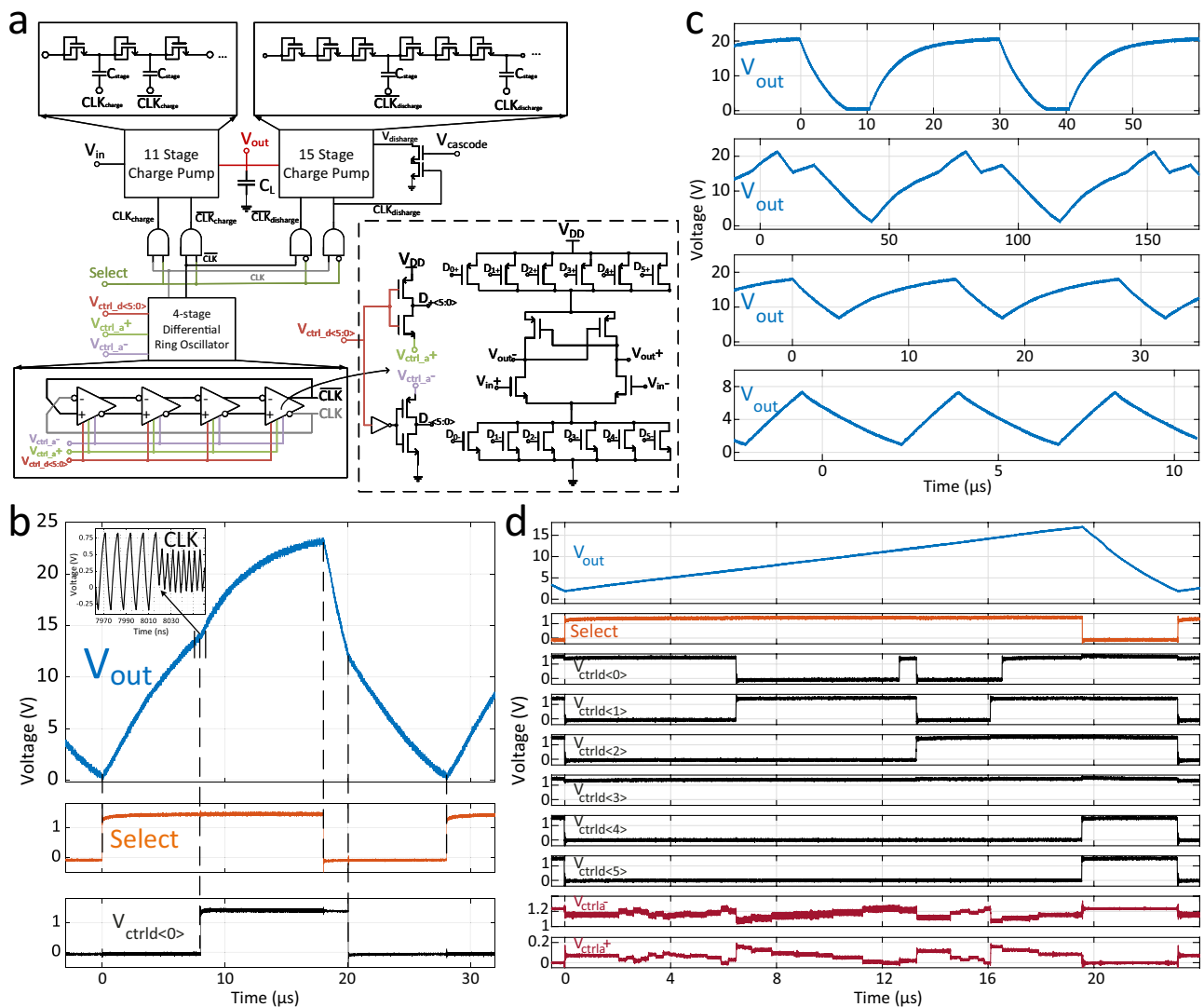


Fig. 2 | High-voltage arbitrary waveform generator integrated circuit, fabricated in a 130-nm SiGe BiCMOS technology. a Schematics of the integrated circuit consisting of a 4-stage voltage-controlled differential ring oscillator which drives charge pump stages to generate high-voltage arbitrary waveforms. **b** Principles of waveform generation demonstrated by the output response to the applied control signals in the time domain. Inset shows the change in oscillation

frequency in response to a frequency control input, from 88 MHz to 208 MHz, which modifies the output waveform. **c** Measured arbitrary waveforms generated by the ASIC with different shapes, amplitudes, periods and offset values. **d** Generation of the linearized sawtooth electrical waveform used in LiDAR measurements. Digital and analog control signals are modulated in the time domain to fine-tune the output.

controlling whether the output voltage increases or decreases. The clocks are applied only to the charging/discharging block during a one-half cycle when the output voltage rises/falls. The oscillator is designed to have a wide frequency range and a high frequency resolution, so as to achieve fine-tuning capability while controlling the waveform. The unit cell of the four-stage ring oscillator has six geometrically sized pairs of NMOS and PMOS (n-type/p-type metal-oxide-semiconductor) transistor loads to control the unit delay. The inputs, V_{ctrlid<5:0>}, can be digitally switched to turn on a pair of NMOS and PMOS loads each, where V_{ctrlid<5>} corresponds to the load with the highest width per length. Using digital inputs, the gate voltage of the PMOS loads is connected to V_{ctrla+} and the NMOS loads to V_{ctrla-}, respectively. These two gate voltages are controlled differentially in an analog fashion, where their sum equals V_{DD} to fine-tune the oscillation frequency. Operating at a supply of 1.2 V, the frequency of the designed oscillator can be set in the range of 6 MHz to 350 MHz, with a tuning control of 2% at lower frequencies and 0.5% at higher frequencies employing 10 mV steps for V_{ctrla+} and V_{ctrla-}.

Figure 2 b illustrates the principles of waveform generation. The output voltage of a charge pump in the time domain shows an exponential response on a capacitive load, where the rise-time depends on the frequency of the applied clocks⁴⁵. Therefore, one can tune the time-domain waveform by changing the clock frequency at pre-determined time points. We can set a digital control input of the VCRO high to decrease the waveform rise time by increasing the clock oscillation frequency, from approximately 88 MHz to 208 MHz. To start the falling edge, we switch ‘Select’ signal low, and the fall time is controlled in the same manner using the oscillator inputs. This allows the HV-AWG ASIC to generate output waveforms with a peak voltage of more than 20 V. The output waveform has a period similar to ‘Select’; ‘Select’ duty cycle also sets the highest and lowest output voltage values. We can produce waveforms with different shapes, amplitudes, frequencies, and offset values when operating the circuit with different VCRO input sequences, as shown in Fig. 2c. Figure 2d shows the generated 45 kHz sawtooth waveform used in our FMCW LiDAR experiments. We linearized the exponential response of the charge pump to obtain a

sawtooth waveform. The voltage control inputs are modified in time to gradually decrease the rise-time, by changing the VCRO frequency within the range of 30–80 MHz. The digital voltages, $V_{\text{ctrlid}<S;0>}$, allow a coarse control of the VCRO causing too abrupt changes in the waveform. The analog voltages, $V_{\text{ctrla+}}$ and $V_{\text{ctrla-}}$, are used in conjunction at smaller time steps, which allows fine-tuning of the optical waveform for higher linearity.

Electro-optic transduction and linearity

Figure 3a demonstrates the electrical waveform generated by the ASIC. The same sawtooth signal was applied to both piezoactuators of the Vernier laser. The heterodyne measurement carried out with an

auxiliary laser shows the time-frequency map of the laser chirp (cf. Fig. 3b). The 15 V electrical signal resulted in >2 GHz optical frequency excursion over a $23 \mu\text{s}$ period. The chirp m parameter of the up-swing used for the ranging equates to ~ 110 THz/s. It ultimately determines the detected beatnote frequency f_{beat} to distance d mapping via $d = c/2m \times f_{\text{beat}}$ where c is the speed of light. In our experiment 1 m of range maps to ~ 1 MHz frequency beatnote for the laser sweep parameters described above.

For the long-range and robust measurement, FMCW LiDAR requires high chirp linearity of the optical waveform¹⁷. To obtain the required AWG signal, we iteratively linearized the optical waveform employing a delayed homodyne detection method⁴⁶. We calculated

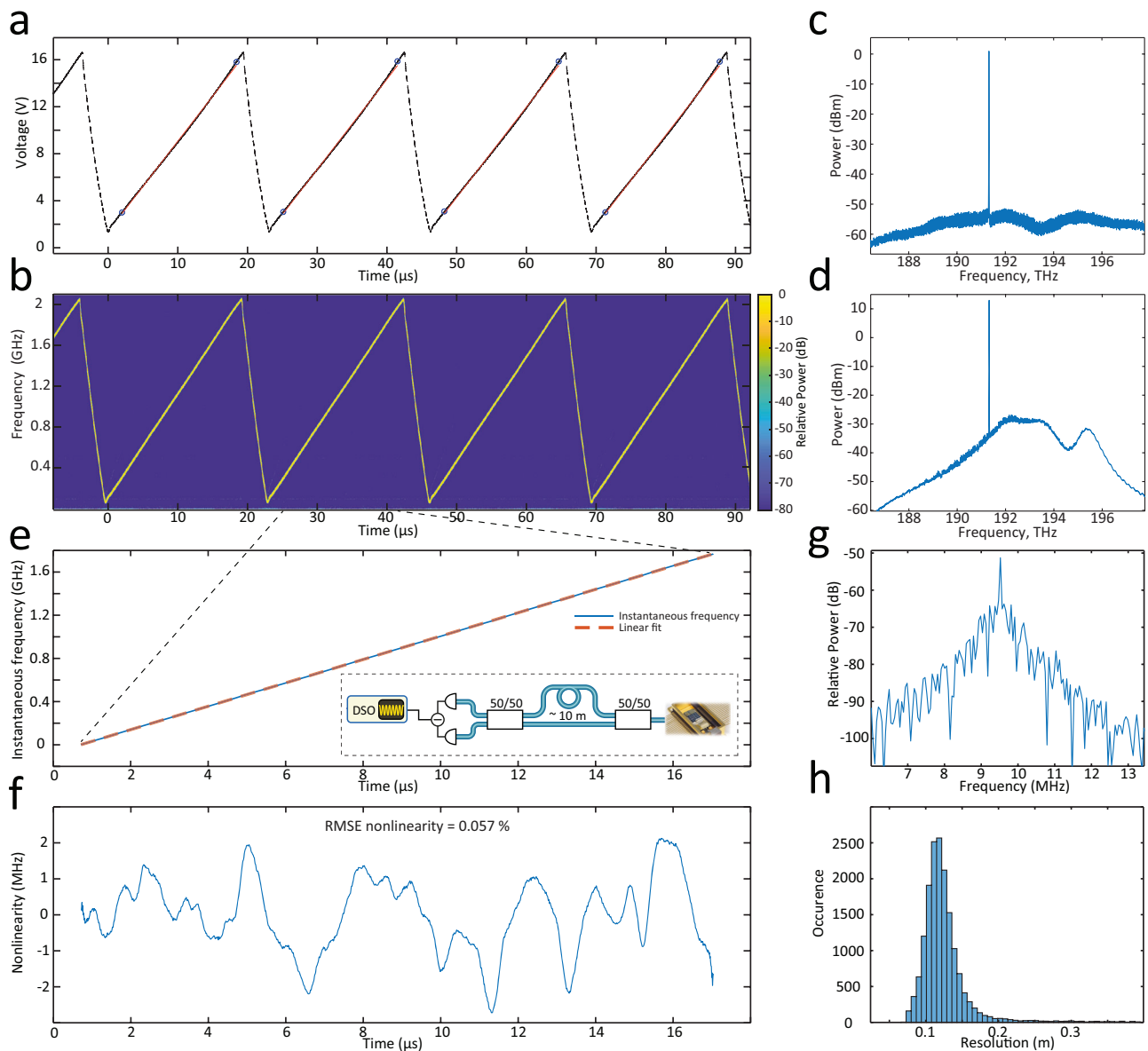


Fig. 3 | Photonic integrated LiDAR source electro-optical transduction and linearity. **a** Electrical waveform generated by the ASIC. Blue circles highlight the segment of $\sim 16 \mu\text{s}$ used for ranging and linearity analysis. The red curve is a linear fit to the given segment. **b** Time-frequency map of the laser chirp obtained via heterodyne detection with auxiliary laser. RBW is set to 10 MHz. **c** Optical spectrum of Vernier laser output featuring 50 dB side mode suppression ratio. **d** Optical spectrum after EDWA with >20 mW optical power. **e** Instantaneous frequency of the optical chirp obtained via delayed homodyne measurement (inset: experimental setup). The red dashed line corresponds to the linear fit. The excursion of the chirp

equates to 1.78 GHz over a $16 \mu\text{s}$ period. **f** Nonlinearity of the laser chirp inferred from (e). RMSE nonlinearity equates to 0.057% with the major chirp deviation from the linear fit lying in the window ± 2 MHz. **g** The frequency beatnote in the delayed homodyne measurement corresponds to the reference MZI delay ~ 10 m. The 90% fraction of the beatnote signal is taken for the Fourier transformation. **h** LiDAR resolution inferred from the FWHM of the MZI beatnotes over $>20,000$ realizations. The most probable resolution value is 11.5 cm, while the native resolution is 9.3 cm corresponding to 1.61 GHz (90% of 1.78 GHz).

the instantaneous frequency of the chirp (cf. Fig. 3e) via Hilbert transformation of the beatnote electric signal. The ASIC architecture allows for fine-tuning the waveform in an arbitrary fashion, therefore we optimized the frequency control inputs of the ASIC to minimize the root mean square error RMSE of the instantaneous frequency. We used a 16 μ s up-rise segment of the chirp for linearity analysis. We note that we described the procedure of finding the needed waveform, which does not require any further feedback during the laser operation. This is in contrast to laser current tuning, where the feedback is essential for linear operation¹⁸.

Figure 3f depicts the chirp nonlinearity or instantaneous frequency deviation from the fitted linear line. The major part of the deviation lies within ± 2 MHz window and exhibits a total nonlinearity of $<0.1\%$. While we optimized the optical waveform, the voltage ramp appeared to have 0.35% linearity and 0.05 V RMSE at an overall 15 V voltage excursion due to the non-ideal electro-optic transduction. We assume the electrical waveform noise limits the linearity of the optical chirp. The VCRO has -1000 oscillations per waveform period, with one one-step output voltage increase occurring at each cycle with charge pumping. The steps change in the range of 20 mV at low output voltages down to 8 mV at higher output voltages. This imposes a limit on

the linearity of 0.05% for 15 V chirps due to quantization error. We envision the increase in clock rate or decrease in voltage step can further improve the nonlinearity affecting ranging resolution and accuracy^{17,47}.

The Fourier transform of the delayed homodyne detection is shown in Fig. 3g. The full width at half maximum (FWHM) of the beatnote determines the resolution of the LiDAR. The beatnote linewidth is nearly Fourier transform limited featuring 60 kHz width. Fig. 3h presents statistics over 2×10^4 measurements. It indicates 11.5 cm resolution ΔR (most probable value) while the native resolution for $B = 1.6$ GHz (90% fraction of 1.78 GHz) excursion chirp equates to 9.3 cm following $\Delta R = c/2B$.

Optical ranging

Figure 4a illustrates the FMCW photonic-electronic LiDAR experimental setup. The Vernier laser was turnkey initiated, and the ASIC pre-configured waveform was subsequently applied to the laser piezo-actuators. The output light was first split into the signal and local oscillator paths. The EDWA chip provided a 13 dB gain and amplified the signal up to 22 mW. The optical spectra before and after the amplification stage are depicted in Fig. 3c, d, respectively. Further

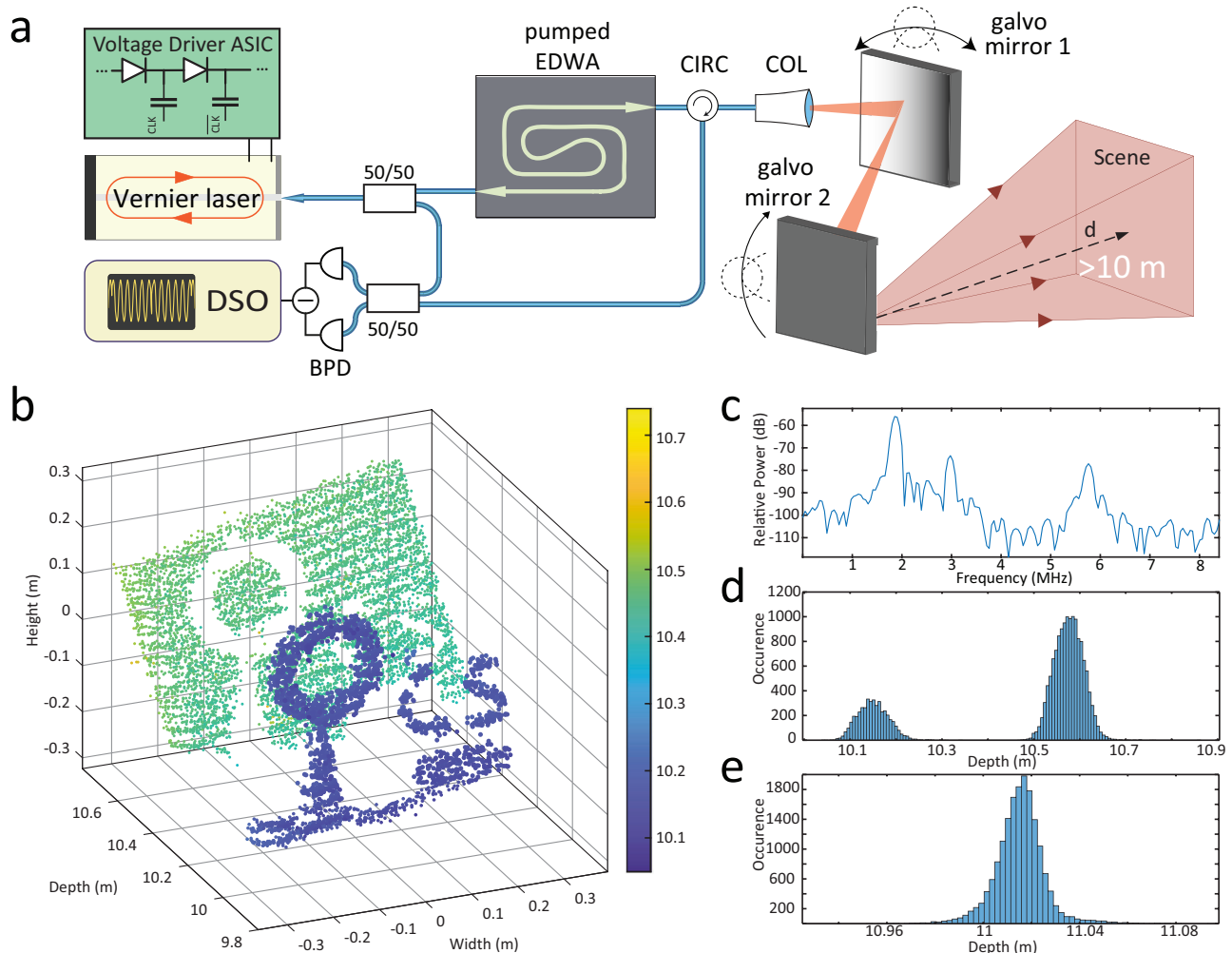


Fig. 4 | Ranging experiment. **a** Schematics of the experimental setup for ranging experiments. The amplified laser chirp scans the target scene via a set of galvo mirrors. A digital sampling oscilloscope (DSO) records the balanced detected beating of the reflected and reference optical signals. CIRC - circulator, COL - collimator, BPD - balanced photodetector. **b** Point cloud consisting of $\sim 10^4$ pixels featuring the doughnut on a cone and C, S letters as a target 10 m away from the

collimator. **c** The Fourier transform over one period, highlighting collimator, circulator and target reflection beatnotes. Blackman-Harris window function was applied to the time trace prior to the Fourier transformation. **d** Detection histogram of **(b)**. **e** Single point imaging depth histogram indicating 1.5 cm precision of the LiDAR source.

amplification is possible with double side pumping of the EDWA chip or by matching the Vernier lasing frequency to the maximum of the gain profile (Liu et al. demonstrated 24 dB off-chip amplification³⁸). We employed a mono-static imaging setup with the same collimator operating as a transmitter and a receiver. Two galvo mirrors scanned the laser beam at 2 Hz vertical and 63 Hz horizontal rates. An optical circulator separated the back-reflected light from the transmitted one, whereafter it was self-heterodyne mixed on a balanced photodetector. The digital oscilloscope sampled the photocurrent at 100 MS/s during 0.25 s acquisition time.

Figure 4b shows the resulting point cloud consisting of ~10,000 pixels. The target comprised a styrofoam doughnut and cone, C and S paper letters, and a flat background placed 10 m away from the collimator (cf. photo of the target in SI). Every pixel was obtained by analyzing a single sawtooth period of 23 μ s. First, the signal was time-gated to the up-swing fraction of the chirp, and then Fourier transformed. Figure 4c depicts a periodogram of the detected signal with the Blackman-Harris window applied. The chirp excursion was obtained from the self-homodyne measurement with an auxiliary interferometer. We performed the Gaussian fitting of the target beatnote to infer the range estimate. We estimated the precision of our setup to be ~1.5 cm derived from the statistics of a single point measurement over $\sim 2 \times 10^4$ realizations. We note that in practical LiDAR applications, it is essential to consider real-world factors such as atmospheric turbulence, including variations in the refractive index along the beam path, as well as the influence of transverse wind^{34,48}.

Discussion

In summary, we have demonstrated an integrated circuit-based coherent LiDAR source. The system-level architecture represents a drop-in frequency-agile laser with ASIC-defined FMCW laser tuning. We showed that a combination of a hybrid integrated Vernier ring laser with fast PZT actuators, a HV-AWG ASIC and an EDWA Si₃N₄ chip, attains 2 GHz frequency sweeps at 50 kHz rate with an output power of more than 20 mW. Our LiDAR engine achieves a 12 cm depth ranging resolution with chirp nonlinearity of less than 0.1%. Employing conventional 2D mechanical galvo mirror scanning, we demonstrated ranging at a 10 m distance with 1.5 cm precision.

The HV-AWG ASIC demonstrated in this work allows for high-voltage arbitrary waveform generation without using a high-voltage supply or an RF power amplifier. Its architecture eliminates the need of high-voltage technologies and additional discrete components, which is limiting for other state-of-the-art solutions. The charge pump-based design can generate output waveforms beyond the voltage rating of the transistors in the technology, so the driver can be implemented in advanced standard CMOS nodes. This is advantageous in terms of power consumption and computational processing capabilities of the system, but the manufacturing cost is typically higher. However, since the design has a small footprint with the possibility of having processing and a high-voltage driver on a single CMOS chip, it supports further integration with the PIC assembly, allowing further miniaturization of the LiDAR engine. Figure 1 in the SI shows the comparison of the proposed HV-AWG with other techniques in the literature, where integration, compactness and versatility are some of the advantages of the architecture. The chirp rate can be further increased from 50 kHz by reducing the parasitic capacitance at the ASIC output by minimizing the packaging or co-integration with the PIC.

Optical power amplification is commonly used in LiDAR demonstrations to achieve the required power levels, since the power output of a standalone laser is often insufficient. On-chip low-noise, high-power optical amplification has been recently made possible in Erbium-implanted Si₃N₄ photonic integrated circuits, showing competitive performance to widely deployed electrically pumped semiconductor optical amplifiers. In contrast to SOAs with picosecond

scale carrier lifetime, the Erbium-based amplifiers enable optical amplification of modulated optical signals with negligible gain non-linearity or channel cross talk, and lower spontaneous emission noise, benefiting from the millisecond scale long excited state lifetime and much smaller emission cross-section, which may be crucial in presence of residual amplitude modulation of optical signals. Although we have demonstrated separate integrated components, we note that the Vernier laser and the EDWA are based on the same Si₃N₄ material. The laser source and the amplifier can be simultaneously integrated on the same photonic chip due to the possibility of selective area Er implantation, providing improved signal-to-noise ratio, higher output power and low fabrication complexity. We used a 1480 nm pump source for Er-ion excitation off-chip. However, it could be hybrid integrated via edge-coupling⁴⁹ or photonic wire bonded⁵⁰.

Finally, we have presented a photonic-electronic integrated coherent ranging source. Comprising integrated laser, HV-AWG ASIC and on-chip amplifier, it could be readily applied to existing LiDAR approaches^{1,2,12} replacing bulk components.

Methods

Vernier ring filter laser operation

In our experiments, the laser operated at a temperature of 26 °C (thermistor resistance 9700 Ω m) and RSOA current of 340 mA, resulting in 3 mW output optical power. We applied around 30 mW of electrical power to microheaters to align resonances of Si₃N₄ microrings. We do not have an on-chip phase shifter section in our laser design, and the tuning range was empirically limited to 3 GHz while the RSOA current was fixed. RSOA is edge coupled to the Si₃N₄ chip, where the coupling waveguide angle of the Si₃N₄ chip is optimized (in simulations) to achieve 20% power transmission (laser output power / nominal RSOA power).

We note that the initial linearization routine is essential for determining the electrical waveform itself and is distinct from the linearization routines applied in postprocessing or feedback. Subsequently, this waveform is stored in memory and reapplied each time. We have observed no degradation in nonlinearity during continuous laser operation over the course of a day, including when the laser is switched off and on with the same operational parameters (such as RSOA current and the current applied to the microheaters used to align the Vernier filter resonances). However, we have observed that making slight adjustments to the laser's operating point can result in a minor degradation of linearity. This effect can be mitigated, and the linearity improved to less than 0.1%, by repeating the calibration procedure.

EDWA chip operation and fabrication

We used lensed fibres to couple the light into the EDWA chip. The 1480 nm pump laser diode was connected via an off-chip 1480/1550 nm coupler. Integrated Si₃N₄ spiral waveguides were fabricated with the photonic damascene process⁵¹. The preform for waveguide structures and filler patterns for stress release was then defined by deep ultra-violet photolithography and transferred into the thermal oxide layer using reactive ion etching (RIE). Thermal treatment at 1250 °C was then applied to reflow the silicon oxide, reducing the roughness caused by the RIE etching⁵², before the preform recesses were filled with stoichiometric Si₃N₄ by LPCVD. An etchback process was performed to roughly planarize the wafer surface and remove the excess Si₃N₄ material. Chemical mechanical polishing (CMP) was then applied to reach the desired waveguide thickness, and create a top surface with sub-nanometer root-mean-square roughness. Using this process, 700 nm-thick Si₃N₄ waveguides buried in a wet oxide cladding but without top cladding were created, which allows for direct Erbium implantation into the waveguide core. The Erbium ion beam energy of 0.955 MeV, 1.416 MeV and 2 MeV and the corresponding fluence of 2.34×10^{15} , 3.17×10^{15} and 4.5×10^{15} ions/cm², respectively, were consecutively applied to the separated passive Si₃N₄ photonic chips. This

process can implant Erbium ions into the Si₃N₄ waveguides (0.7 × 2.1 μm² cross-section) with a maximum doping depth of ca. 400 nm from the top surface and achieve an overlap factor of ca. 50%. The doped Si₃N₄ was then annealed at 1000° C in O₂ under atmosphere pressure for 1 hour to heal the implantation defects and optically activate the doped Erbium ions. The measured lifetime of the first excited state of doped Erbium ions is ca. 3.4 ms. Higher annealing temperature could lead to Erbium ion precipitations in the silica cladding³⁷. The Erbium ion implantation of the Si₃N₄ photonic chips was performed at the University of Surrey Ion Beam Centre via commercial service.

HV-AWG ASIC operation

The design was fabricated in a standard 130-nm SiGe BiCMOS technology, where only CMOS transistors were used. The chip measures 1.17–1.07 mm². The total active area of the design, i.e. excluding decoupling caps and IO pads, is approximately 35,000 μm². The charge pump is implemented with diode-connected isolated thick oxide NMOS transistors and metal-insulator-metal (MiM) capacitors. V_{in} and V_{cascode} were biased at V_{DD} = 3.3V. The 15-stage charge pump has three diode-connected transistors in each stage, so as to set V_{discharge} to V_{out} - 45V_{th,n} as V_{out} rises during the charging phase. A cascode transistor is also introduced at V_{discharge}, so that a voltage up to 2V_{DD} can be tolerated at this node. This ensures that V_{out} can safely reach more than 20 volts without reaching the breakdown of the discharge transistors, given that the capacitors and NMOS-to-bulk isolation are within breakdown limits as well. For the measurements presented, the output of the CMOS chip was fed to an external unity-gain voltage buffer whose output was measured and/or used to drive the actuators. Load capacitance at chip output was measured at 26 pF. The printed circuit board used for controlling the ASIC is shown in SI Fig. 2.

Data availability

Data used to produce the plots within this paper is available at <https://doi.org/10.5281/zenodo.10668672>. All other data used in this study are available from the corresponding authors upon request.

Code availability

Code used to produce the plots within this paper is available at <https://doi.org/10.5281/zenodo.10668672>.

References

- Rogers, C. et al. A universal 3d imaging sensor on a silicon photonics platform. *Nature* **590**, 256–261 (2021).
- Zhang, G. et al. Demonstration of high output power DBR laser integrated with SOA for the FMCW LiDAR system. *Opt. Express* **30**, 2599–2609 (2022).
- Poulton, C. V. et al. Coherent LiDAR With an 8,192-Element Optical Phased Array and Driving Laser. *IEEE J. Sel. Top. Quantum Electron.* **28**, 1–8 (2022).
- Urmson, C. et al. Autonomous driving in urban environments: Boss and the urban challenge. *J. Field Robot.* **25**, 425–466 (2008).
- Bostick, H. A carbon dioxide laser radar system. *IEEE J. Quantum Electron.* **3**, 232–232 (1967).
- Pierrottet, D. et al. Linear FMCW laser radar for precision range and vector velocity measurements. *MRS Online Proceedings Library Archive.* **1076**, K04–O6 (2008).
- Martin, A. et al. Photonic integrated circuit-based FMCW coherent LiDAR. *J. Lightwave Technol.* **36**, 4640–4645 (2018).
- Baba, T. et al. Silicon Photonics FMCW LiDAR Chip With a Slow-Light Grating Beam Scanner. *IEEE J. Sel. Top. Quantum Electron.* **28**, 1–8 (2022).
- Bogaerts, W., Dwivedi, S., Jansen, R., Rottenberg, X. & Dahlem, M. S. A 2D Pixelated Optical Beam Scanner Controlled by the Laser Wavelength. *IEEE J. Sel. Top. Quantum Electron.* **27**, 1–12 (2021).
- Muñoz, P. et al. Scalable Switched Slab Coupler Based Optical Phased Array on Silicon Nitride. *IEEE J. Sel. Top. Quantum Electron.* **28**, 1–16 (2022).
- Zhang, X., Kwon, K., Henriksson, J., Luo, J. & Wu, M. C. A large-scale microelectromechanical-systems-based silicon photonics LiDAR. *Nature* **603**, 253–258 (2022).
- Poulton, C. V. et al. Long-range lidar and free-space data communication with high-performance optical phased arrays. *IEEE J. Sel. Top. Quantum Electron.* **25**, 1–8 (2019).
- Isaac, B. J., Song, B., Pinna, S., Coldren, L. A. & Klamkin, J. Indium Phosphide Photonic Integrated Circuit Transceiver for FMCW LiDAR. *IEEE J. Sel. Top. Quantum Electron.* **25**, 1–7 (2019).
- Sayyah, K. et al. Fully Integrated FMCW LiDAR Optical Engine on a Single Silicon Chip. *J. Lightwave Technol.* **40**, 2763–2772 (2022).
- Amann, M.-C. Phase noise limited resolution of coherent LiDAR using widely tunable laser diodes. *Electron. Lett.* **28**, 1694–1696 (1992).
- Karlsson, C. J. & Olsson, F. A. A. Linearization of the frequency sweep of a frequency-modulated continuous-wave semiconductor laser radar and the resulting ranging performance. *Appl. Opt.* **38**, 3376–3386 (1999).
- Zhang, X., Pouls, J. & Wu, M. C. Laser frequency sweep linearization by iterative learning pre-distortion for FMCW LiDAR. *Opt. Express* **27**, 9965–9974 (2019).
- Behroozpour, B. et al. Electronic-Photonic Integrated Circuit for 3D Microimaging. *IEEE J. Solid-State Circuits* **52**, 161–172 (2017).
- Tran, M. A., Huang, D. & Bowers, J. E. Tutorial on narrow linewidth tunable semiconductor lasers using Si/III-V heterogeneous integration. *APL Photonics* **4**, 111101 (2019).
- Jin, W. et al. Hertz-linewidth semiconductor lasers using CMOS-ready ultra-high-Q microresonators. *Nat. Photonics* **15**, 346–353 (2021).
- Lihachev, G. et al. Low-noise frequency-agile photonic integrated lasers for coherent ranging. *Nat. Commun.* **13**, 3522 (2022).
- Li, M. et al. Integrated Pockels laser. *Nat. Commun.* **13**, 5344 (2022).
- Snigirev, V. et al. Ultrafast tunable lasers using lithium niobate integrated photonics. *Nature* **615**, 411–417 (2023).
- Li, Z. et al. High density lithium niobate photonic integrated circuits. *Nat. Commun.* **14**, 4856 (2023).
- Zhang, J. et al. Fundamental charge noise in electro-optic photonic integrated circuits. <http://arxiv.org/abs/2308.15404> (2023).
- Rees, A. V. et al. Ring resonator enhanced mode-hop-free wavelength tuning of an integrated extended-cavity laser. *Opt. Express* **28**, 5669–5683 (2020).
- Chen, C. et al. Hybrid integrated Si₃N₄ external cavity laser with high power and narrow linewidth. *Opt. Express.* **31**, 26078–26091 (2023).
- Siddharth, A. et al. Hertz-linewidth and frequency-agile photonic integrated extended-DBR lasers. <https://arxiv.org/abs/2306.03184v2> (2023).
- Lihachev, G. et al. Frequency agile photonic integrated external cavity laser. <http://arxiv.org/abs/2303.00425> (2023).
- Pulskamp, J. et al. Monolithically Integrated Piezomems SP2T Switch and Contour-Mode Filters. In *2009 IEEE 22nd International Conference on Micro Electro Mechanical Systems*, 900–903 (2009).
- Satyan, N., Vasilyev, A., Rakuljic, G., Leyva, V. & Yariv, A. Precise control of broadband frequency chirps using optoelectronic feedback. *Opt. Express* **17**, 15991–15999 (2009).
- Xi, J., Huo, L., Li, J. & Li, X. Generic real-time uniform K-space sampling method for high-speed swept-Source optical coherence tomography. *Opt. Express* **18**, 9511–9517 (2010).
- Okano, M. & Chong, C. Swept source lidar: simultaneous FMCW ranging and nonmechanical beam steering with a wideband swept source. *Opt. Express* **28**, 23898–23915 (2020).

34. Fenevrou, P. et al. Frequency-modulated multifunction lidar for anemometry, range finding, and velocimetry–1. theory and signal processing. *Appl. Opt.* **56**, 9663–9675 (2017).
35. Axelsson, S. Noise radar using random phase and frequency modulation. *IEEE Trans. Geosci. Remote Sens.* **42**, 2370–2384 (2004).
36. Wang, J. Y. Heterodyne laser radar-SNR from a diffuse target containing multiple glints. *Appl. Opt.* **21**, 464–476 (1982).
37. Polman, A., Jacobson, D. C., Eaglesham, D. J., Kistler, R. C. & Poate, J. M. Optical doping of waveguide materials by MeV Er implantation. *J. Appl. Phys.* **70**, 3778–3784 (1991).
38. Liu, Y. et al. A photonic integrated circuit-based erbium-doped amplifier. *Science* **376**, 1309–1313 (2022).
39. Pollnau, M. Rare-earth-ion-doped channel waveguide lasers on silicon. *IEEE J. Sel. Top. Quantum Electron.* **21**, 414–425 (2015).
40. Lee, J. et al. A 36-channel auto-calibrated front-end ASIC for a pmu-based miniaturized 3-d ultrasound system. *IEEE J. Solid-State Circuits* **56**, 1910–1923 (2021).
41. Jung, G. et al. Single-chip reduced-wire active catheter system with programmable transmit beamforming and receive time-division multiplexing for intracardiac echocardiography. In *2018 IEEE International Solid - State Circuits Conference - (ISSCC)*, 188–190 (2018).
42. Sooksood, K., Noorsal, E., Becker, J. & Ortmanns, M. A neural stimulator front-end with arbitrary pulse shape, hv compliance and adaptive supply requiring 0.05mm² in 0.35um hvcmos. In *2011 IEEE International Solid-State Circuits Conference*, 306–308 (2011).
43. Zhang, I. & Zbinden, P. Advances in ingaas/inp single-photon detector systems for quantum communication. *Light.: Sci. Appl.* **4**, e286–e286 (2015).
44. Dragonas, F. A., Neretti, G., Sanjeevikumar, P. & Grandi, G. High-voltage high-frequency arbitrary waveform multilevel generator for dbd plasma actuators. *IEEE Trans. Ind. Appl.* **51**, 3334–3342 (2015).
45. Palumbo, G. & Pappalardo, D. Charge pump circuits: An overview on design strategies and topologies. *IEEE Circuits Syst. Mag.* **10**, 31–45 (2010).
46. Ahn, T.-J. & Kim, D. Y. Analysis of nonlinear frequency sweep in high-speed tunable laser sources using a self-homodyne measurement and hilbert transformation. *Appl. Opt.* **46**, 2394–2400 (2007).
47. Qiao, L., Sun, D., Zhang, X. & Zhao, Y. Linearity Requirement for a Linear Frequency Modulation Lidar. *Opt. Rev.* **6**, 160–162 (1999).
48. Frehlich, R. G. & Kavaya, M. J. Coherent laser radar performance for general atmospheric refractive turbulence. *Appl. Opt.* **30**, 5325–5352 (1991).
49. Zhu, Y. & Zhu, L. Narrow-linewidth, tunable external cavity dual-band diode lasers through InP/GaAs-Si₃N₄ hybrid integration. *Opt. Express* **27**, 2354–2362 (2019).
50. Blaicher, M. et al. Hybrid multi-chip assembly of optical communication engines by in situ 3D nano-lithography. *Light.: Sci. Appl.* **9**, 1–11 (2020).
51. Pfeiffer, M. H. P. et al. Photonic damascene process for low-loss, high-confinement silicon nitride waveguides. *IEEE J. Sel. Top. Quantum Electron.* **24**, 1–11 (2018).
52. Pfeiffer, M. H. P. et al. Ultra-smooth silicon nitride waveguides based on the damascene reflow process: fabrication and loss origins. *Optica* **5**, 884 (2018).

Acknowledgements

This publication was supported by Contract W911NF2102048 (NINJA LASER) from the Defense Advanced Research Projects Agency (DARPA), Microsystems Technology Office (MTO), as well as the Swiss National Science Foundation (SNSF) through grant number 211728 (BRIDGE). A.L.

acknowledges support from the European Space Technology Centre with ESA Contract No. 4000133568/20/NL/MH/hm. This work also received funding from the EU H2020 research and innovation programme under the Marie Skłodowska-Curie grant agreement No. 101033663 (RaMSoM), as well as the Horizon Europe EIC Transition grant agreement no. 101113302 (MAGNIFY).

Author contributions

H.K.Y. designed the ASIC. A.B. and A.V. performed hybrid packaging of the laser. Y.L., Z.Q. and X.J. developed the EDWA chip. A.L. and H.K.Y. performed the measurements with assistance from A.B., G.L. and Y.L. A.L. performed the data analysis. A.L. and H.K.Y. wrote the manuscript with input from all authors. T.J.K., E.C. and S.B. supervised the work.

Competing interests

The views, opinions and/or findings expressed are those of the authors and should not be interpreted as representing the official views or policies of the Department of Defense or the U.S. Government. Dr. Sunil Bhave performed this research at Purdue University prior to becoming a DARPA program manager. T.J.K. is a co-founder and shareholder of LiGenTec SA, a foundry commercializing Si₃N₄ photonic integrated circuits. T.J.K., A.V. are co-founders and shareholders of DEEPLIGHT SA and A.B. is a shareholder of DEEPLIGHT SA, a start-up company commercializing Si₃N₄ photonic integrated circuits based frequency agile low noise lasers. There are no other competing interests.

Additional information

Supplementary information The online version contains supplementary material available at <https://doi.org/10.1038/s41467-024-47478-z>.

Correspondence and requests for materials should be addressed to Edoardo Charbon or Tobias J. Kippenberg.

Peer review information *Nature Communications* thanks Xingjun Wang, Chang-Seok Kim and the other, anonymous, reviewer(s) for their contribution to the peer review of this work. A peer review file is available.

Reprints and permissions information is available at <http://www.nature.com/reprints>

Publisher's note Springer Nature remains neutral with regard to jurisdictional claims in published maps and institutional affiliations.

Open Access This article is licensed under a Creative Commons Attribution 4.0 International License, which permits use, sharing, adaptation, distribution and reproduction in any medium or format, as long as you give appropriate credit to the original author(s) and the source, provide a link to the Creative Commons licence, and indicate if changes were made. The images or other third party material in this article are included in the article's Creative Commons licence, unless indicated otherwise in a credit line to the material. If material is not included in the article's Creative Commons licence and your intended use is not permitted by statutory regulation or exceeds the permitted use, you will need to obtain permission directly from the copyright holder. To view a copy of this licence, visit <http://creativecommons.org/licenses/by/4.0/>.

© The Author(s) 2024